

# Quantification of Molecular Interactions in Living Cells in Real Time using a Membrane Protein Nanopattern

Andreas Michael Reichmuth, Mirjam Zimmermann, Florian Wilhelm, Andreas Frutiger, Yves Blickenstorfer, Christof Fattinger, Maria Waldhoer,\* and János Vörös\*



Cite This: <https://dx.doi.org/10.1021/acs.analchem.0c00987>



Read Online

ACCESS |



Metrics & More

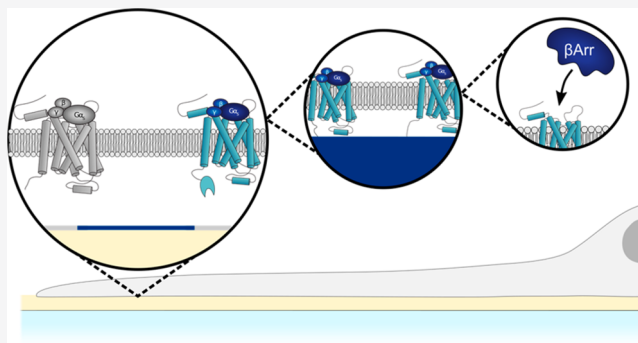


Article Recommendations



Supporting Information

**ABSTRACT:** Molecular processes within cells have traditionally been studied with biochemical methods due to their high degree of specificity and ease of use. In recent years, cell-based assays have gained more and more popularity since they facilitate the extraction of mode of action, phenotypic, and toxicity information. However, to provide specificity, cellular assays rely heavily on biomolecular labels and tags while label-free cell-based assays only offer holistic information about a bulk property of the investigated cells. Here, we introduce a cell-based assay for protein–protein interaction analysis. We achieve specificity by spatially ordering a membrane protein of interest into a coherent pattern of fully functional membrane proteins on the surface of an optical sensor. Thereby, molecular interactions with the coherently ordered membrane proteins become visible in real time, while nonspecific interactions and holistic changes within the living cell remain invisible. Due to its unbiased nature, this new cell-based detection method presents itself as an invaluable tool for cell signaling research and drug discovery.



interactions and holistic changes within the living cell remain invisible. Due to its unbiased nature, this new cell-based detection method presents itself as an invaluable tool for cell signaling research and drug discovery.

The ability to examine living cells in a physiologically relevant context is crucial to the understanding of cellular processes and emanating drug discovery efforts. While traditional biochemical assays are well-established and provide high molecular specificity, they often fail to report functional and cytological insight. Live cell assays, on the other hand, facilitate studies on stimuli-induced toxicity and phenotypic responses. For mode of action and pathway analysis, whole cell assays rely on fluorescent labels and molecular tags. These enable insight into specific protein activity, reveal distinct intracellular second messengers, or report the expression of a gene under control of a signaling cascade.<sup>1–9</sup> State-of-the-art whole cell assays thus require considerable biomolecular modifications that can significantly alter cellular physiology by affecting the conformation of single proteins or entire complexes, altering the concentration of certain proteins, and are sometimes disturbed by the compounds to be tested.<sup>10</sup> Therefore, label-free whole cell assays, promising straightforward measurements without the need for recurring assay development and validation, were quickly embraced to complement the traditional label-assisted technologies.<sup>11</sup> The Epic system was one of the first commercial label-free systems for monitoring cellular signaling pathways in real time.<sup>12</sup> In principle, similar to surface plasmon resonance, it utilizes a resonance waveguide grating biosensor to monitor small refractive index changes in the evanescent field above a sensor chip by means of refractometry. The penetration depth of the

evanescent wave into the sample defines the volume in which the sensor is sensitive to changes of the shape or the bulk refractive index of adherent cells on the sensor surface.<sup>13,14</sup> Redistribution of any cellular content within this sensing volume results in an overall change in the refractive index. However, this detection process is inherently cross-sensitive, since both specific and nonspecific molecular processes as well as morphological changes in the cell or fluctuations in temperature and buffer composition evoke refractive index changes. This is why intricate molecular interactions within cells cannot be deconvolved spatiotemporally by this refractometric sensor method.<sup>15</sup>

Here, we introduce “cell-based focal molography” (“cell-based molography” in short), a new, quantitative, whole cell assay method which uses focal molography to overcome the specificity constraint of label-free refractometric assays.<sup>16–18</sup> This diffractometric method uses a spatially defined sensing pattern of membrane proteins within adherent cells to eliminate disturbing cross-sensitivities in the assay. Focal

Received: March 5, 2020

Accepted: May 14, 2020

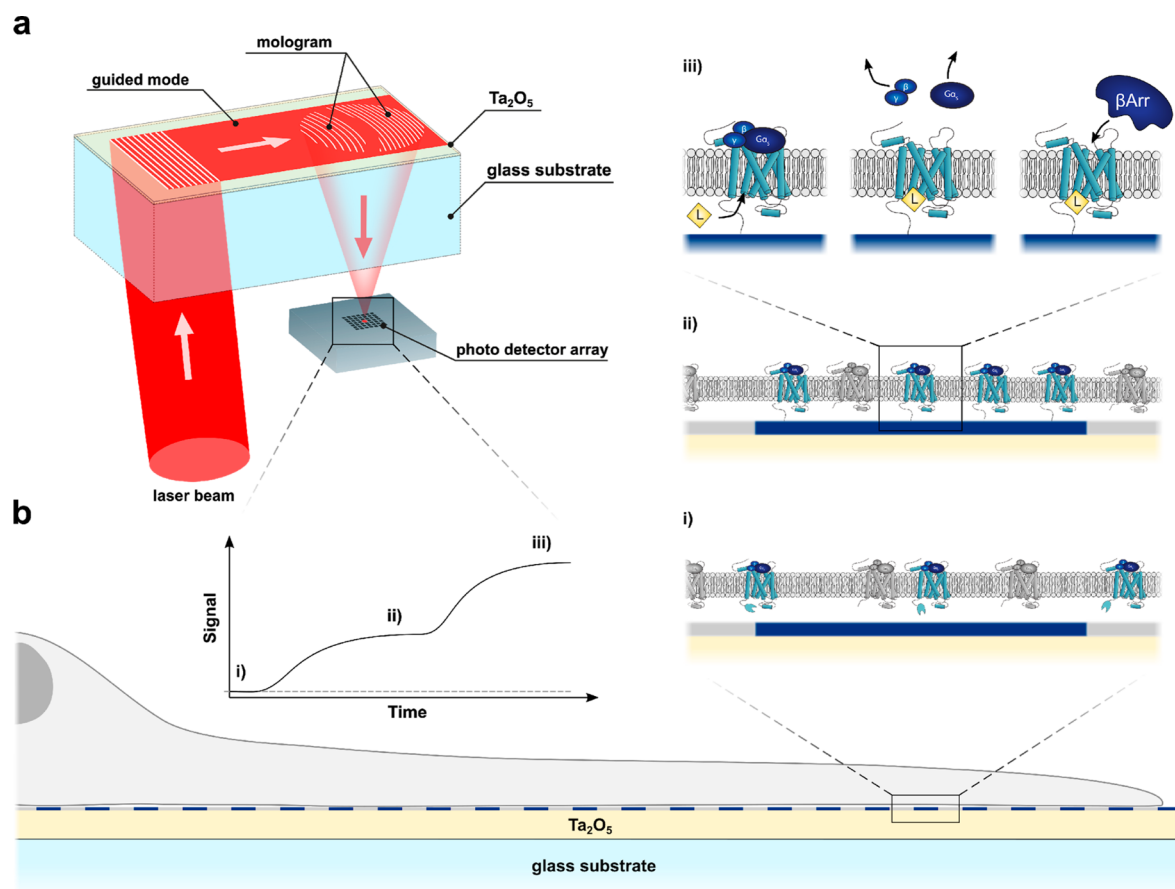


**Figure 1.** Principle of focal molography and illustration of the working principle of cell-based molography. (a) A single-mode optical waveguide with graft copolymer layer serves as a sensor chip for focal molography. The guided mode is diffracted at the biomolecules comprising the mologram and forms a diffraction-limited focal spot. Molecules that bind to the mologram contribute to the light intensity in the focal spot, whereas other molecules in the sample do not contribute to this signal. The light intensity scales quadratically with the number of molecules bound to the mologram. The time course of the light intensity is monitored with a photodetector array. (b) Reactive immersion lithography (RIL) is used to generate a template mologram capable of ordering the membrane protein of interest in the adherent cells on the mologram (Supporting Information Figure S1). The autoreactive SNAP-tag protein is fused to the extracellular side of the membrane protein of interest, here a transmembrane spanning, G protein coupled receptor. The SNAP-tag permits one to arrange the target receptor to the template mologram on the sensor chip by covalent binding to the SNAP-tag substrate. Cells are plated onto the sensor chip. (i) Target and off-target proteins expressed in cells diffuse freely within the plasma membrane. (ii) The randomly distributed target receptors are localized to the mologram on the chip via the extracellular SNAP-tag, leading to a spatial organization of the receptors within the cell membrane. As a result, the mologram is transferred from the surface of the chip into the plasma membrane of the cell, establishing a transmembrane mologram. The number of receptors that are arranged in this fashion can be controlled by the number and therefore the density of SNAP-tag binding sites on the template mologram. Unbound as well as off-target receptors stay randomly distributed. (iii) Refractive index changes at the arranged proteins of interest change the molographic signal. Such refractive index changes are caused either by a local mass change through ligand binding (left), dissociation (middle), or association (right) of cytosolic proteins but also by local changes in ion concentration caused by water or ion influx through a membrane channel. Other molecular interactions, e.g., binding at off-target membrane proteins do not contribute to the molographic signal because they are incoherent.

molography is a method for molecular interaction analysis in crude samples. In contrast to refractometric optical sensors, focal molography is insensitive to nonspecific molecular interactions. This unique property is achieved with a special 2D nanopattern of molecular binding sites, termed mologram (Figure 1a). A mologram is designed such that molecules bound to it diffract light constructively into a focal spot. The intensity of the focused light in this spot is measured to quantify the amount of bound molecules.<sup>16,18</sup> Off-target molecules that do not bind to the binding sites of the mologram, yet are highly abundant in biologically relevant samples, do not diffract into the focal spot of the mologram. Thus, they do not contribute to the measured light intensity.

We now elaborate the basic principle of cell-based molography: Cells plated onto a molographic sensor chip

spread and adhere under standard tissue culture conditions. The targeted membrane protein in the plasma membrane of the living cells is aligned by a “template mologram” on the surface of the chip. In doing so, the membrane protein molecules transfer the molographic pattern from the substrate of the chip to the inside of the cell, forming a “transmembrane mologram” (Figure 1b). The transmembrane mologram has the following key characteristics: The coherently arranged membrane protein molecules under study remain in their natural environment but become visible through their coherent arrangement inside the cell membrane. They create a diffraction-limited spot of light, the focus of the transmembrane mologram. Molecules interacting with their intra- or extracellular domains diffract light into this spot. Changes in the intensity of this spot are used to quantify molecular binding

to the targeted membrane protein in the transmembrane mologram. In contrast, off-target proteins that do not interact with the coherently arranged membrane protein and other molecules distributed randomly throughout the cell do not affect the molographic signal. As a result, cell-based molography enables real-time quantification of specific biomolecular interactions of the targeted membrane protein in living cells. The evanescent field of the guided mode limits the sensitive volume above the surface of the sensor chip to a thin layer of approximately 80 nm thickness. Within this sensitive volume, cell-based focal molography probes all interactions of molecules with the transmembrane protein in the transmembrane mologram. Thereby, this new analytical method enables investigations of transmembrane proteins in their natural environment. In contrast to the classical methods for label-free analysis of membrane proteins in living cells (refractometric sensors, cellular dielectric spectroscopy, or digital holographic microscopy),<sup>13,14,19,20</sup> cell-based molography is not disturbed by minute holistic refractive index changes in the penetration depth of the evanescent field caused by, e.g., temperature fluctuations, changes in buffer composition and concentration, and small changes of the shape of the adherent cells. Note, traditionally the term label-free is used to describe the analyte molecules as opposed to the immobilized binders. While the classical methods mentioned above are truly “modification-free”, cell-based molography still uses a molecular modification on the receptor to facilitate alignment to the template mologram. Molecules interacting with the receptor however are free of any modifications and expressed endogenously.

This work presents, for the first time, the experimental realization of cell-based molography using the  $\beta$ 2-adrenergic receptor ( $\beta$ 2AR), a well-studied G-protein coupled receptor (GPCR).<sup>21–23</sup> First, we demonstrate the establishment of a transmembrane mologram of  $\beta$ 2ARs in living cells. We then exemplify the functionality of this technique by measuring molecular interactions in real time at the intracellular side of the receptor. Second, we show that cell-based molography only records specific molecular interactions with the receptor of interest and is insensitive to any other molecular interactions. Third, we perform traditional fluorescence-based assays simultaneously with cell-based molography to identify the intracellular interaction partner  $\beta$ -arrestin-2 to be responsible for the molographic response. Finally, we prove that the spatial arrangement of the receptor molecules into a mologram does not influence their biological function.

## MATERIALS AND METHODS

Cell culture medium DMEM high glucose (4.5 g/L) with L-glutamine (BioConcept, Switzerland), Lipofectamine 2000, Opti-MEM I (1x) Versene 1:5000 (1x), Hank's balanced salt solution (HBSS), and Zeozin were purchased from Life Technologies Europe (Zug, Switzerland). HEPES was from GERBU Biotechnik GmbH (Heidelberg, Germany); fetal bovine serum (FBS) was purchased from Sigma-Aldrich Chemie GmbH (Buchs SG, Switzerland). G418 was from InvivoGen (San Diego, CA, USA), tissue culture flasks from VWR International GmbH (Dietikon, Switzerland), and Biofil tissue culture plate 24 wells were from Axon Lab AG (Baden-Dättwil, Switzerland). Corning Costar sterile black 96-well plates, clear bottom, TC treated, poly-D-lysine coated were from Vitaris AG (Baar, Switzerland), custom coated CulturPlate-96, white opaque 96-well microplate, Sterile and

Tissue Culture Treated and ViewPlate-96, white 96-well microplate with Clear Bottom, Sterile and Tissue Culture Treated were from PerkinElmer (Schwerzenbach, Switzerland). TPP 6-well tissue culture plates were from Faust Laborbedarf AG (Schaffhausen, Switzerland) Coelenterazine 400a, Deep Blue C (DBC) was purchased from Cayman Chemical (Ann Arbor, MI, United States). The GRGDSPGSC-(DBCO) peptide was custom synthesized by LifeTein, LLC (Somerset, NJ, USA). BG-GLA-NHS was obtained from BioConcept Ltd. (Alschwil, Switzerland). Azido-PEG4-NHS was obtained from Jena Bioscience (Jena, Germany). The PAA-g-PEG-NH-PhSNPPOC copolymer, used as a biocompatible coating, was a kind gift of Roche (Basel, Switzerland). Isoproterenol hydrochloride and formoterol hemifumarate was purchased from Tocris Bioscience (Bristol, U.K.). ICI 118,551 hydrochloride, fluorescein-O'-acetic acid and all other chemicals were purchased from Sigma-Aldrich Chemie GmbH (Buchs SG, Switzerland). Zeptosens thin-film optical waveguides with a 145 nm Ta<sub>2</sub>O<sub>5</sub> layer with the in- and out-coupling gratings covered with a 1  $\mu$ m thick layer of SiO<sub>2</sub> by IMT Masken and Teilungen AG (Greifensee, Switzerland) were a kind gift of Roche.

**Plasmids.** The mPlum- $\beta$ Arr2 coding sequence was a kind gift of Philipp Berger (Villigen, Switzerland) and recloned into a pcDNA3 expression vector. The GFP- $\beta$ Arr2 coding sequence was kindly provided by Hans Bräuner-Osborne (Copenhagen, Denmark) and was recloned into a pEGFP (Clontech) expression vector. The  $\beta$ 2AR-RLuc8 plasmid was a kind gift of Nevin Lambert (Augusta University, Georgia).

**Cell Lines and Cell Culture.** A HEK293 cell line stably expressing the SNAP- $\beta$ 2-adrenergic receptor (referred to as SNAP- $\beta$ 2AR) was purchased from Cisbio (Codolet, France). HEK293 stably overexpressing SNAP- $\beta$ 2AR in  $\Delta\beta$ arr1/2 cells<sup>24</sup> and the corresponding wild-type HEK293 cells were most kindly provided by Dr. Asuka Inoue, Tohoku University. All HEK293 cells were cultured in DMEM supplemented with 10% (v/v) fetal bovine serum and 600  $\mu$ g/mL G418 with 5% CO<sub>2</sub> at 37 °C.

**Preparation of Sensor Chips.** Thin-film optical waveguides were treated with a similar protocol as reported previously.<sup>17</sup> In short, waveguides were washed with 0.1% aqueous Tween 20, followed by ultrasound-assisted washing in Milli-Q water, isopropanol, and toluene. The chips were then soaked in warm Hellmanex III for 1 min, thoroughly rinsed with Milli-Q water, and cleaned with highly oxidizing Piranha solution (7:3 H<sub>2</sub>SO<sub>4</sub>/H<sub>2</sub>O<sub>2</sub>) for 30 min. After excessive washing with Milli-Q water, the chips were centrifuge-dried at 800 rcf for 2 min and activated by oxygen plasma. After plasma treatment, the chips were immediately immersed in the PAA-g-PEG-NH-PhSNPPOC graft copolymer coating solution (0.1 mg/mL in 1 mM HEPES, pH 7.4) for 60 min. To fully passivate the layer, the chips were washed with Milli-Q water and ethanol and immersed in a 25 mM solution of methyl chloroformate in anhydrous acetonitrile containing 2 equiv of *N,N*-diisopropylethylamine for 5 min. The coated chips were washed with ethanol and Milli-Q water and blow-dried by a nitrogen jet. Prepared sensor chips were stored in the dark at 4 °C until further use.

**Preparation of Template Molograms.** Molograms were prepared according to the standard RIL process described previously.<sup>17,25</sup> Briefly, a copolymer-coated sensor chip was placed in a custom holder. The phase mask used to generate the molograms was aligned using an alignment help, and the

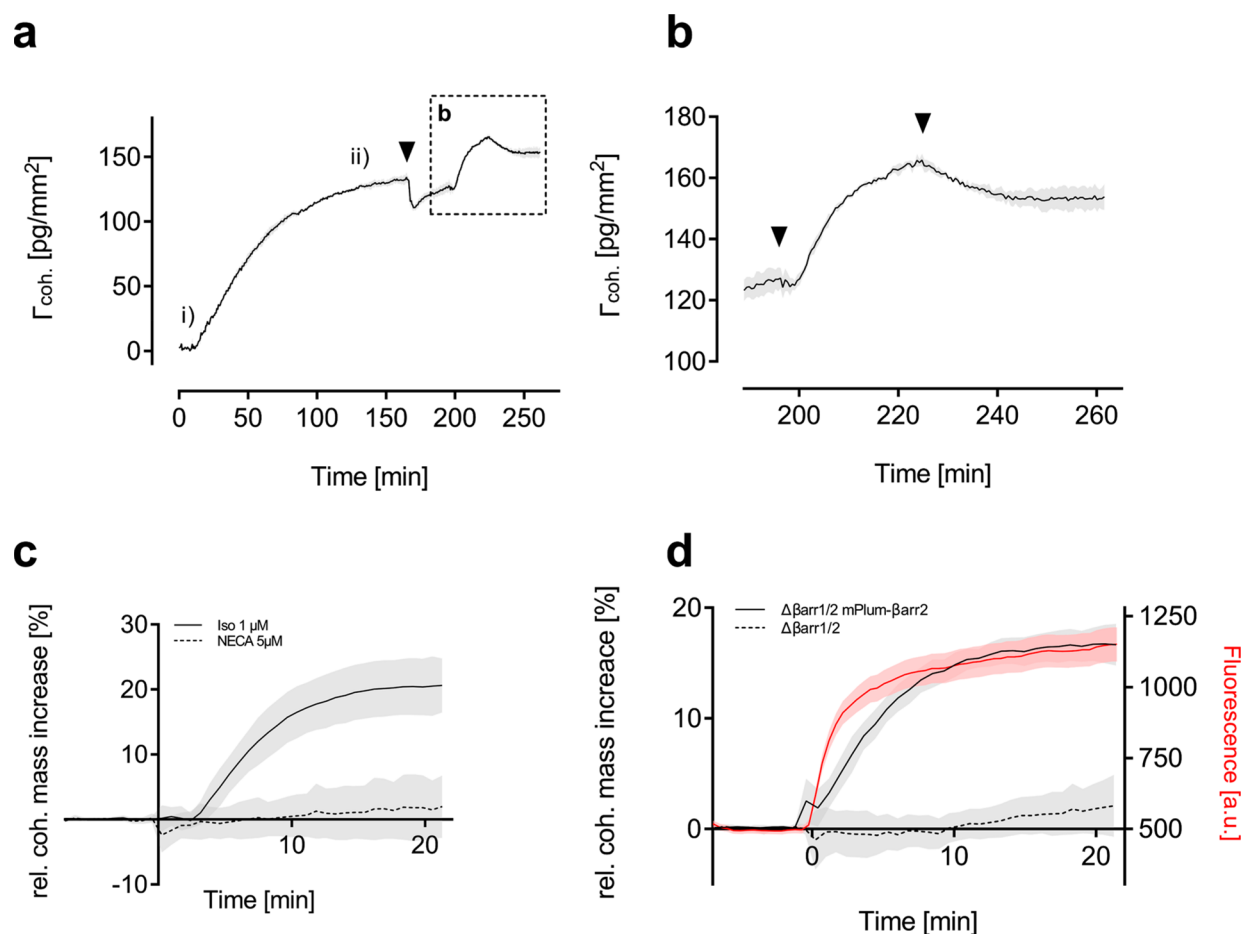


**Figure 2.** Formation of a functional SNAP- $\beta$ 2AR transmembrane mologram in HEK293 cells. (a) (i) SNAP- $\beta$ 2AR HEK293 cells are plated on a sensor chip with previously employed template molograms. (ii) The GPCRs arrange within the cell membrane over the course of about 150 min while the molographic signal is recorded. Once the transmembrane mologram is formed, the medium is exchanged for the assay buffer (black arrow). (b) Stimulation of the SNAP- $\beta$ 2ARs with 1  $\mu$ M isoproterenol (first arrow) shows an increase in the molographic signal, which is partially reversed by the addition of a 10  $\mu$ M amount of the competitive antagonist ICI 118,551 (second arrow). Displayed in panels a and b are the mean equivalent coherent mass density modulations of four individual molograms of one representative experiment with the barely visible standard deviation (s.d.) as a gray ribbon. (c) SNAP- $\beta$ 2AR HEK293 cells were stimulated with 5  $\mu$ M NECA to activate off-target A2A/A2B adenosine receptors endogenously expressed in HEK293 cells. A negligible molographic response was observed compared to stimulation of the target receptor with 1  $\mu$ M isoproterenol. Data represent mean  $\pm$  s.d. of  $n \geq 3$  individual experiments. (d) For the deconvolution of the SNAP- $\beta$ 2AR coupling partner,  $\Delta\beta$ arr1/2 cells were stimulated with 1  $\mu$ M isoproterenol showing no response (dashed black line). However, a transient transfection of mPlum- $\beta$ arr2 into the same cell line led to a recovery of the molographic signal (solid black line) upon stimulation. Simultaneous read out of the mPlum-mediated fluorescence at the mologram (red line) is overlaid on the right y-axis. Molographic data represent the drift corrected, baseline normalized mean  $\pm$  s.d. of  $n \geq 3$  biological replicates. Fluorescence data represent the mean background corrected fluorescence  $\pm$  s.d. of  $n = 3$  individual experiments.

gap between the chip and phase mask was filled with a solution of 0.1% (v/v) hydroxylamine in DMSO. The photolithographic exposure was conducted at 405 nm with a dose of 2000 mJ/cm<sup>2</sup> in a custom-built setup. After illumination the chip was washed with isopropanol and Milli-Q water and the activated ridges were functionalized with 1 mM amine reactive SNAP-tag substrate (BG-GLA-NHS), to which the SNAP-tag protein can covalently bind. In order to increase cell adhesion to the chip, remaining PhSNPPOC groups were removed by flood exposure and the remaining free binding sites were functionalized with the hetero-biofunctional cross-linker azido-PEG4-NHS. Finally, the chip was incubated with an azide reactive aqueous solution of 0.5 mM GRGDSFGSC-(DBCO) overnight, washed with isopropanol and Milli-Q water, and dried with a jet of nitrogen. This process is schematically displayed in Supporting Information Figure S1. The setup and

phasemask used to generate template molograms were a kind gift of Roche.

**Molographic Cell Measurements.** SNAP- $\beta$ 2AR cells were grown to 60–80% confluency in T25 culture flasks, washed twice with warm phosphate-buffered saline (PBS), incubated with 1 $\times$  Versene for 5 min, and resuspended in cell culture medium. In order to decrease baseline signal contributions from nonfunctional cellular debris, the cells were centrifuged at 50 rcf for 1 min and resuspended in culture media two times sequentially. The cells were seeded to reach confluency on the molographic chip in an incubation chamber containing 500  $\mu$ L of cell culture media. Cells were only seeded when viability exceeded 90%, as determined by a Countess automated cell counter (Invitrogen). Except for the real-time establishment of the transmembrane mologram (Figure 2a), seeded cells were kept in a CO<sub>2</sub> incubator at 37  $^{\circ}$ C for 2 h to allow cell adherence to the sensor chip (and

covalent interaction of the SNAP-tag on the  $\beta$ 2AR with the SNAP-tag substrate on the chip). The incubation chamber containing the cells was then washed twice with warm HBSS buffer (supplemented with 20 mM HEPES, pH 7.4) adjusted for DMSO, and transferred to a modified F3000 ZeptoReader (Zeptosens), which was kept at 35 °C. The molographic chip was then allowed to temperature equilibrate inside the ZeptoReader for 5–10 min before performing the assay. For all molographic assays, the signal was monitored for 7 min (baseline measurement) before careful substitution of the buffer with buffer containing the  $\beta$ 2AR ligand and monitored for another 21 min thereafter. For the real-time establishment of the transmembrane mologram experiment (Figure 2a), the molographic measurement was performed in cell culture media supplemented with 20 mM HEPES, pH 7.4. Once the mologram was established, the culture medium was carefully exchanged with HBSS buffer (supplemented with 20 mM HEPES, pH 7.4).

Typical instrument parameters for molographic signal acquisition were as follows: one image was acquired every 10 s using the 635 nm laser with an integration time of 0.25–1 s depending on the intensity of the initial signal and a gray filter value of 0.001 in the illumination path of the ZeptoReader. For the quasi-simultaneous fluorescent readout (Figure 2d), the image plane was adjusted to the surface of the thin-film waveguide after every molographic image and the fluorescent signal was measured using the red filter of the ZeptoReader. For real-time evaluation of molographic and fluorescent signal, automation (AutoHotkey) and evaluation (MATLAB) scripts were used.<sup>17</sup>

**Transient Transfections of SNAP- $\beta$ 2AR  $\Delta\beta$ arr1/2 Cells with mPlum- $\beta$ Arr2.** SNAP- $\beta$ 2AR  $\Delta\beta$ arr1/2 cells were seeded in 6-well plates at 600–800k cells/well in 2 mL of culture media. Cells were transfected with 2  $\mu$ g of mPlum- $\beta$ Arr2 DNA per well using Lipofectamine 2000 24 h prior to the experiment.

**Arrestin Recruitment Assays.** A BRET assay was performed essentially as described in ref 26. In brief,  $\beta$ 2AR was C-terminally tagged with RLuc8 (BRET donor) and the  $\beta$ -arrestin-2 was N-terminally tagged with GFP (BRET acceptor). RLuc8 catalyzes oxidation of its substrate (Coelenterazine 400A), which results in the emission of photons ( $\lambda_{\text{max}} = 410$  nm) which will excite the GFP if it is in close proximity. HEK293 cells were transiently transfected with BRET donor and acceptor constructs with Lipofectamine2000 according to manufacturer's protocol (briefly, HEK293 cells were seeded at a density of 500k cells/well in a sterile cell culture 6-well plate; 24 h later cells were transfected using 2  $\mu$ g of DNA, 6  $\mu$ L of Lipofectamine, 150  $\mu$ L of OptiMEM/6-well, and the BRET acceptor compared to BRET donor construct at a ratio of 1:10). Twenty-four hours after transfection, the cells were transferred into a poly-L-lysine-coated, white, sterile 96-well microplate at a density of 50k/well and cultured overnight. Cells were incubated in 90  $\mu$ L of HBSS (supplemented with 20 mM HEPES, pH 7.4 and 50  $\mu$ M Coelenterazine 400A), and baselines were measured on a PHERAstar FSX from BMG Labtech (Ortenberg, Germany). Cells were stimulated with isoproterenol and formoterol at the concentrations indicated. The isoproterenol- and formoterol-induced recruitment of GFP- $\beta$ Arr2 to the  $\beta$ 2AR-RLuc8 brings GFP into close proximity of the BRET donor, which results in its excitation and emission of light at 515 nm. BRET ratios (515 nm/410 nm) were detected with the optic module BRET2 plus (515-

30, 410-80) and normalized to 10  $\mu$ M isoproterenol and plotted as a function of time for 30 min post-stimulation. pEC<sub>50</sub> values were calculated from concentration–response curves with area under the curve (AUC) vs ligand concentrations plotted in GraphPad Prism 8.

**Data Analysis and Calculations.** For the quantitative, real-time establishment of a transmembrane mologram, the equivalent coherent mass modulation was obtained via an algorithm that computes the power in the waveguide from the scattered background intensity of the waveguide mode as described in ref 18. The anisotropy of the scattering was assumed to be 0.054,<sup>18</sup> the damping constant was computed for every chip and mologram field (3–6 dB/cm), and the numerical aperture of the ZeptoReader is 0.33. Since the ZeptoReader cannot resolve the Airy disk, the measured signal (arbitrary units) was divided by the expected Airy disk area to obtain a quantity that was proportional to the average intensity in the Airy disk. The quantity proportional to the background intensity was computed from the background signal (arbitrary units) by dividing it by the pixel size of the ZeptoReader (12.5  $\times$  12.5  $\mu\text{m}^2$ ). The ratio of these two quantities was then used in eq 11 of ref 18 with the necessary scaling factors to obtain the equivalent coherent mass density from the average intensity in the Airy disk. The algorithm was implemented in MATLAB as well as in Python.

The number of GPCRs per cell measured in Figure 2a was derived as follows. The equivalent coherent mass density was multiplied with the area of the mologram footprint to receive the coherent mass. We assumed that the template mologram was covered by about 1000 cells. However, because of the central curved recess area, only about 80% of the cells establish a transmembrane mologram. The coherent mass was thus divided by 800 cells to receive the coherent mass per cell. To account for imperfect alignment of the receptors, the coherent mass per cell has to be divided by the analyte efficiency (0.24)<sup>25</sup> to receive the total mass of the receptors per cell. Assuming a molecular weight of 66 kDa per receptor, we obtain approximately 775,000  $\beta$ 2ARs. From this, the average distance between the receptors can be calculated by dividing the number of receptors per cell by the footprint of a single cell. Taking the inverse of the square root then leads to the average distance between individual receptors.

For all molographic assays, the square root of the raw molographic signal was taken. The baseline was then fitted linearly and used to detrend the signal (this was done since the transmembrane mologram was not equally well established between individual experiments). Data were then displayed as a fractional change compared to the baseline.

For the BRET arrestin recruitment assay and the molographic dose response, the concentration–response curves with AUC vs ligand concentrations were fitted using the nonlinear regression “log(inhibitor) vs response (three parameters)” in GraphPad Prism 8 to calculate the pEC<sub>50</sub> values.

## RESULTS AND DISCUSSION

**GPCRs Alignment in the Cell Membrane to Form a Functional Mologram.** To perform a GPCR assay molographically, the receptor of interest freely diffusing within the cell membrane needs to be aligned into a molographic pattern. To this end, a template mologram was created on the surface of a sensor chip using the previously established RIL process (see refs 17 and 25 and Supporting Information Figure S1).

SNAP- $\beta$ 2ARs expressed in HEK293 cells were bound to the template mologram using the N-terminal SNAP-tag. The SNAP- $\beta$ 2ARs transfer the diffractive nanopattern from the surface of the chip into the cell membrane, while their intra- and extracellular binding sites constitute a transmembrane mologram, which is sensitive to molecular interactions. The generation of a SNAP- $\beta$ 2AR transmembrane mologram (Figure 2a) with a diameter of 400  $\mu$ m requires approximately 1000 cells covering the template mologram. Initially, all SNAP- $\beta$ 2ARs are distributed randomly within the cell membrane and no signal is detected (Figure 2a(i)). Over the course of 150 min, the SNAP- $\beta$ 2ARs align on the chip via their extracellular SNAP-tags to form a transmembrane mologram (Figure 2a(ii)). Thanks to its real-time and quantitative nature, molography can also determine this coherently arranged mass during transmembrane mologram formation.<sup>18</sup> Since the uniformly distributed molecules in the plasma membrane do not significantly contribute to the signal generation (Supporting Information Figure S2, gray curve), the observed 130  $\text{pg}/\text{mm}^2$  equivalent coherent mass density (Figure 2a) thus corresponds to approximately 775,000 GPCRs per cell with an average distance between the receptors in the mologram of approximately 15 nm. The minimal number of GPCRs required for a molographic signal on this experimental setup is approximately 60,000 or  $\sim 10 \text{ pg}/\text{mm}^2$  as seen in Figure 2a. The average distance of the receptors can be tuned by changing the density of SNAP-tag binding sites on the template mologram.

In order to demonstrate functionality of the newly established mologram in the HEK293 SNAP- $\beta$ 2AR cells, cells were stimulated with 1  $\mu$ M of the agonist isoproterenol (first arrow in Figure 2b). The molographic signal increased over the course of 20 min, corresponding to the recruitment and thus alignment of additional mass at the receptor. No decrease in signal intensity could be observed during these first 20 min post-stimulation, suggesting that the recruited molecule did not leave the receptors and that receptors were not internalized by the cell. This was expected, as SNAP- $\beta$ 2ARs are covalently bound to the chip.

Upon addition of 10  $\mu$ M of the competitive antagonist/inverse agonist ICI 118,551 (second arrow in Figure 2b), a decline of the molographic trace could be observed, indicating that part of the GPCRs reversibly bound their intracellular targets. In a stably established transmembrane mologram, any change in mass at the receptor complex results in a change of the molographic signal intensity. In principle, this means that the binding of a small drug molecule should also be measurable, but practically the fractional mass increase at the receptor was still within the noise level and could thus not be detected. Similarly, G-protein association to and dissociation from the intracellular portion of the receptor, expected to start about 300 ms after receptor activation, should be visible on the curve.<sup>27</sup> Surprisingly, we often observed a minute signal dip within the first minute after receptor activation (small dip following the first arrow in Figure 2b), which might be indicative of G-protein dissociation. However, this is rapidly followed by a signal increase indicative of arrestin binding which could mask this process. Therefore, current temporal resolution does not allow for a conclusive association of this tiny signal dip with G-protein signaling.

Overall, the results presented in Figure 2a,b demonstrate the successful establishment of a GPCR-mediated, functional

transmembrane mologram, sensitive to (drug-induced) intracellular molecular interactions.

**Cell-Based Molography Insensitive to Off-Target Receptor Signaling.** Compared to other cellular assays, focal molography is practically not affected by off-target molecules. Cell-based molography is no different; i.e., the recorded molographic signal is truly receptor specific with no contribution from off-target receptors or morphological changes of the studied cell per se. To exemplify this property, we stimulated the off-target adenosine A2A/A2B receptors endogenously expressed in HEK293 cells with the high-affinity agonist 5'-N-ethylcarboxamidoadenosine (NECA) and monitored the molographic response from the target SNAP- $\beta$ 2AR (Figure 2c).<sup>28</sup> In contrast to other assays (see cAMP assay in Supporting Information Figure S4), we did not observe any significant change in the molographic signal upon activation of the adenosine A2A/A2B receptors with NECA (Figure 2c, dashed line). This is due to the diffractive origin of the molographic signal, meaning that only receptors precisely arranged to the mologram (in this case  $\beta$ 2ARs) and molecules interacting with these receptors diffract light constructively into the focal spot and thus contribute to the signal. On the other hand, all randomly distributed receptors (e.g., the A2A/A2B here) or freely diffusing molecules within the evanescent field scatter light uniformly and do not contribute to the signal. Similarly, morphological changes to the cell body resulting from GPCR activation or non-ideal environmental conditions are incoherent in their nature and therefore do not contribute to the molographic signal either.<sup>29</sup> This is in sharp contrast to other assays that record both specific and nonspecific molecular interactions and are sensitive to morphological changes of the cell.<sup>12,14,30,31</sup> As a consequence, cell-based molography can not only answer the question of whether GPCRs are activated or not but also provide insight into the temporal occurrence and precise kinetics of the specific molecular interaction with the receptor of interest.

**Simultaneous Fluorescent Assays Allowing for the Deconvolution of GPCR Coupling Partners.** As we can exclude signal contributions from off-target receptors, the recorded molographic response directly correlates with the molecular weight and number of the recruited species (proteins) to the receptor. Knowing that the molecular weight of the SNAP- $\beta$ 2AR is approximately 66 kDa and assuming that at high ligand concentrations all coherently arranged receptors are activated, the measured response of  $\sim 20\%$  (Figure 2c, solid curve) of the  $\beta$ 2AR complex mass corresponds to around 13 kDa for the recruited species. This is far from the expected molecular weight of most proteins known to interact with GPCRs, suggesting that not all receptors have recruited an intracellular protein.<sup>32,33</sup> However, if we know the intracellular protein responsible for the molographic signal increase, we can determine the fraction of occupied receptors. An obvious candidate is  $\beta$ -arrestin-2, an important regulatory protein interacting with the  $\beta$ 2AR which, among others, is involved in receptor desensitization within minutes after receptor activation.<sup>32–34</sup> To test this hypothesis, we formed a SNAP- $\beta$ 2AR mologram in HEK293 cells devoid of  $\beta$ -arrestin-2 ( $\Delta\beta$ arr1/2).<sup>35,36</sup> Upon stimulation of the SNAP- $\beta$ 2AR  $\Delta\beta$ arr1/2 cells with 1  $\mu$ M isoproterenol (see Supporting Information Figure S3 for cAMP assay testing the functionality of SNAP- $\beta$ 2ARs in  $\Delta\beta$ arr1/2 cells), no increase in the molographic signal could be observed (Figure 2d, dashed curve). However, when  $\Delta\beta$ arr1/2 cells were transiently

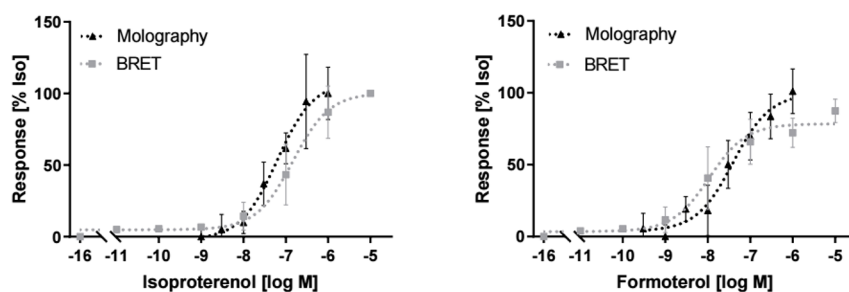


**Figure 3.** Cell-based molography compared to classical BRET arrestin recruitment assay. For the molographic assay, cells were treated with increasing concentration of isoproterenol (left) or formoterol (right). The molographic signal was normalized to 1  $\mu$ M isoproterenol (=100%). For the BRET arrestin-2 recruitment assay, HEK293 cells transiently coexpressing  $\beta$ 2AR-RLuc8 and GFP-arrestin-2 WT constructs were treated with coelenterazine 400A and stimulated with increasing concentration of isoproterenol (left) or formoterol (right). The BRET ratio (515 nm/410 nm) was normalized to 10  $\mu$ M isoproterenol. For both assays the area under the curve (AUC) was plotted as a function of agonist concentrations. Data for molography represent mean  $\pm$  s.d. of  $n \geq 3$  individual experiments. Data for the BRET assay represent mean  $\pm$  s.d. of three individual experiments carried out in duplicate.

transfected with a fluorescently labeled  $\beta$ -arrestin-2 (mPlum- $\beta$ Arr2), the molographic response to stimulation with 1  $\mu$ M isoproterenol was recovered (Figure 2d, solid black curve). To verify whether it was indeed the mPlum- $\beta$ Arr2 protein being recruited to the SNAP- $\beta$ 2AR mologram, we simultaneously acquired mPlum-mediated fluorescence at the mologram (Figure 2d, solid red curve) which confirmed the recruitment of fluorescently labeled  $\beta$ -arrestin-2. Compared to cell-based molography, the fluorescence signal depicts faster  $\beta$ -arrestin-2 binding to the SNAP- $\beta$ 2AR (Figure 2d, black curve vs red curve). This slight discrepancy between fluorescent and molographic signal might be due to the different specificity of the two methods. Isoproterenol also activates endogenous  $\beta$ 2ARs and other isoforms of the  $\beta$ -adrenergic receptor class present in HEK293 cells.<sup>28,37</sup> Simultaneous activation of these GPCRs thus leads to more labeled arrestin being recruited to the cell membrane, which results in faster kinetics for the fluorescent measurement, compared to the molographic signal which only detects arrestin recruited to the SNAP- $\beta$ 2AR receptor. Having identified the intracellular interaction partner responsible for the molographic signal increase, we can now come back to the question of receptor occupancy. With a molecular weight of 66 kDa for the receptor and 47 kDa for  $\beta$ -arrestin-2 the relative coherent mass increase for complete saturation of receptors would need to be  $\sim$ 71%. The observed response (Figure 2c, solid curve) thus suggests that only  $\sim$ 28% of the receptors have actually recruited arrestin. However, we stress that the experiments have been carried out in a highly overexpressing  $\beta$ 2AR cell line; hence, the ratio between GPCRs and arrestins is likely skewed in favor of the receptor. At this point we return to the discussion of G-protein signaling. Due to the absence of  $\beta$ -arrestin-2 in  $\Delta\beta$ arr1/2 cells there is no longer any competitive mass transport that could mask G-protein action in the molographic signal. However, upon stimulation of  $\Delta\beta$ arr1/2 cells with 1  $\mu$ M isoproterenol (Figure 2d, dashed curve) we observe a negligible drop in the molographic signal. Because G-protein signaling is expected to start within the first  $\sim$ 300 ms and persist for several minutes,<sup>27</sup> this suggests that the associated G-proteins stay in close proximity to the receptor (i.e., they stay coherently arranged with the receptor).

**No Mologram Formation Interference with GPCR Function.** The formation of a transmembrane mologram requires that the receptors of interest, here the SNAP- $\beta$ 2ARs, assemble into a precise nanopattern in the cell membrane. To

show that this arrangement of the receptors did not affect their functionality, we compared the molographic signal to a classical arrestin recruitment assay based on BRET.<sup>2,38</sup> HEK293 cells transiently coexpressing  $\beta$ 2AR-RLuc8 and GFP- $\beta$ -arrestin were stimulated with increasing concentrations of isoproterenol or formoterol, and arrestin recruitment kinetics were measured (see Supporting Information Figure S5). The concentration-dependent increase in the molographic signal, caused by arrestin recruitment (Figure 3, black triangles), was virtually identical to the concentration-dependent increase of the fluorescent signal (Figure 3, gray squares) measured in the BRET-recruitment assay for both agonists. Consequently, cell-based molography adequately represents the biological function of the receptor of interest. The reason for this nonperturbing nature of molography is simple: proteins are minimally biologically altered and merely brought into a well-defined order. It is the spatial organization of the receptors of interest into a diffractive grating and the ability of the receptors to likewise organize cytosolic proteins that distinctly reveals molecular processes which were previously masked by the chaotic environment of the cell. With an average distance in the order of 15 nm between individual GPCRs, other molecules and membrane proteins are not perturbed and stay naturally disorganized within the cell.

## CONCLUSIONS

In summary, we have demonstrated the realization of cell-based molography as a new quantitative whole cell assay. Cell-based molography distinguishes itself from other whole cell assays in that it is visualizing molecular interactions specific to the receptor of interest and is insensitive to holistic changes in the system. This unique signal allows for the temporal quantification and thus deconvolution of complex signal transduction processes in whole cells. While cytosolic and membrane bound proteins can still freely access the investigated GPCRs, the impact of the extracellular label and the covalent arrangement of the receptor to the mologram remains unclear. The covalent arrangement of target receptors to the template mologram prevents internalization which is required for receptor desensitization. Moreover, the lack of lateral mobility could negatively impact receptor oligomerization which has been shown to be functionally relevant.<sup>39</sup> At present we could not conclusively resolve small molecule binding or G-protein signaling molographically due to instrumental limitations. However, we foresee that further

improving the sensitivity and temporal resolution of the system used for cell-based molography will allow for even deeper insight into the precise temporal succession of molecules and proteins interacting with the receptor of interest. Along this line we have already demonstrated a limit of detection below 300 fg/mm<sup>2</sup> with subsecond time resolution for streptavidin binding to biotin.<sup>18</sup>

Owing to its potential for miniaturization and parallelization, we anticipate cell-based molography to be of great importance for receptor deorphanization. Here, focal molography requires no a priori knowledge of signaling pathways, yet delivers a result that is unspoiled from off-target GPCRs.<sup>40</sup> Since cell-based molography is insensitive to the composition of the assay medium, it could overcome the limitation of ligand availability as assays could be performed directly in tissue lysates without the need of purification.<sup>41</sup> However, while cell-based molography does not alter endogenous receptor modifying proteins that might be required for receptor activation, it would remain unclear if labeling and arrangement impairs target orphan receptor function.<sup>42,43</sup>

Finally, the concept of cell-based molography is not only limited to GPCRs and cells. It could be extended to other membrane bound proteins such as receptor tyrosine kinases, immune receptors, or possibly even ion channels provided they can be tagged extracellularly. While we have used an autoreactive SNAP-tag for this study, any other molecular tag could be used including HA-tag, biotin, and others. Since focal molography is largely insensitive to the composition of the assay medium, the concept can readily be extended to (crude) membrane preps or unilamellar vesicles. Such “cell-free” settings allow for more stringent control over the complexity of the investigated system.

## ■ ASSOCIATED CONTENT

### SI Supporting Information

The Supporting Information is available free of charge at <https://pubs.acs.org/doi/10.1021/acs.analchem.0c00987>.

Additional schematics and control experiments of the methodology (Figures S1 and S2); additional control experiments with fluorescent techniques (Figures S3–S5) (PDF)

## ■ AUTHOR INFORMATION

### Corresponding Authors

János Vörös – Laboratory of Biosensors and Bioelectronics, Institute of Biomedical Engineering, University and ETH Zurich, 8092 Zurich, Switzerland; [orcid.org/0000-0001-6054-6230](https://orcid.org/0000-0001-6054-6230); Email: [janos.voros@biomed.ee.ethz.ch](mailto:janos.voros@biomed.ee.ethz.ch)

Maria Waldhoer – InterAx Biotech, PARK innovAARE, 5234 Villigen, Switzerland; Email: [waldhoer@interaxbiotech.com](mailto:waldhoer@interaxbiotech.com)

### Authors

Andreas Michael Reichmuth – Laboratory of Biosensors and Bioelectronics, Institute of Biomedical Engineering, University and ETH Zurich, 8092 Zurich, Switzerland

Mirjam Zimmermann – InterAx Biotech, PARK innovAARE, 5234 Villigen, Switzerland

Florian Wilhelm – InterAx Biotech, PARK innovAARE, 5234 Villigen, Switzerland; Department of Biosystems Science and Engineering, ETH Zurich, 4058 Basel, Switzerland

Andreas Frutiger – Laboratory of Biosensors and Bioelectronics, Institute of Biomedical Engineering, University and ETH Zurich, 8092 Zurich, Switzerland

Yves Blickenstorfer – Laboratory of Biosensors and Bioelectronics, Institute of Biomedical Engineering, University and ETH Zurich, 8092 Zurich, Switzerland

Christof Fattiger – Roche Pharma Research and Early Development, Roche Innovation Center Basel, 4070 Basel, Switzerland

Complete contact information is available at: <https://pubs.acs.org/10.1021/acs.analchem.0c00987>

### Author Contributions

J.V. and C.F. contributed to the original idea of ordering membrane proteins to a template mologram. A.M.R. came up with the idea of establishing a transmembrane mologram to be able to study both intra- and extracellular molecular interactions. M.W. conceptualized the study and together with A.M.R. and M.Z. designed the experiments. Molographic experiments were performed by A.M.R. Comparative experiments with other techniques were performed by M.Z. and F.W. A.F. and Y.B. wrote custom scripts for data evaluation. M.W. and A.M.R. conceptualized the manuscript. A.M.R. wrote the manuscript with the help of M.Z. and C.F. All authors were involved in commenting and reviewing the manuscript.

### Notes

The authors declare no competing financial interest.

## ■ ACKNOWLEDGMENTS

We thank Philipp Berger and Hans Bräuner Osborne for kindly providing the arrestin constructs and Nevin Lambert for kindly providing the  $\beta$ 2AR-RLuc8 construct. We further thank Dr. Asuka Inoue, Tohoku University for providing the knockout cell line and Jesper M. Mathiesen for the EPAC cell lines (Supporting Information). We thank Nadine Dobberstein for technical assistance and Betty Xiong for early exploratory experiments. We further thank Gebhard Schertler, Volker Gatterdam, and Elena Cambria for valuable discussions and feedback.

## ■ REFERENCES

- (1) Akerboom, J.; Chen, T.-W.; Wardill, T. J.; Tian, L.; Marvin, J. S.; Mutlu, S.; Calderón, N. C.; Esposti, F.; Borghuis, B. G.; Sun, X. R.; Gordus, A.; Orger, M. B.; Portugues, R.; Engert, F.; Macklin, J. J.; Filosa, A.; Aggarwal, A.; Kerr, R. A.; Takagi, R.; Kracun, S.; Shigetomi, E.; Khakh, B. S.; Baier, H.; Lagnado, L.; Wang, S. S.-H.; Bargmann, C. I.; Kimmel, B. E.; Jayaraman, V.; Svoboda, K.; Kim, D. S.; Schreiner, E. R.; Looger, L. L. *J. Neurosci.* **2012**, *32* (40), 13819–13840.
- (2) Kamal, M.; Marquez, M.; Vauthier, V.; Leloire, A.; Froguel, P.; Jockers, R.; Couturier, C. *Biotechnol. J.* **2009**, *4* (9), 1337–1344.
- (3) Cheng, Z.; Garvin, D.; Paguio, A.; Stecha, P.; Wood, K.; Fan, F. *Curr. Chem. Genomics* **2010**, *4*, 84–91.
- (4) Oakley, R. H.; Hudson, C. C.; Cruickshank, R. D.; Meyers, D. M.; Payne, R. E., Jr.; Rhem, S. M.; Loomis, C. R. *Assay Drug Dev. Technol.* **2002**, *1* (1), 21–30.
- (5) Middleton, R. J.; Kellam, B. *Curr. Opin. Chem. Biol.* **2005**, *9* (5), 517–525.
- (6) Kenakin, T. P. *Nat. Rev. Drug Discovery* **2009**, *8* (8), 617–626.
- (7) Williams, C. *Nat. Rev. Drug Discovery* **2004**, *3* (2), 125–135.
- (8) Hamdan, F. F.; Audet, M.; Garneau, P.; Pelletier, J.; Bouvier, M. *J. Biomol. Screening* **2005**, *10* (5), 463–475.
- (9) Barnea, G.; Strapps, W.; Herrada, G.; Berman, Y.; Ong, J.; Kloss, B.; Axel, R.; Lee, K. J. *Proc. Natl. Acad. Sci. U. S. A.* **2008**, *105* (1), 64–69.

- (10) Gribbon, P.; Sewing, A. *Drug Discovery Today* **2003**, *8* (22), 1035–1043.
- (11) Rocheville, M.; Jerman, J. C. *Curr. Opin. Pharmacol.* **2009**, *9* (5), 643–649.
- (12) Fang, Y.; Ferrie, A. M.; Fontaine, N. H.; Yuen, P. K. *Anal. Chem.* **2005**, *77* (17), 5720–5725.
- (13) Fang, Y.; Ferrie, A. M.; Fontaine, N. H.; Mauro, J.; Balakrishnan, J. *Biophys. J.* **2006**, *91* (5), 1925–1940.
- (14) Cunningham, B. T.; Li, P.; Schulz, S.; Lin, B.; Baird, C.; Gerstenmaier, J.; Genick, C.; Wang, F.; Fine, E.; Laing, L. *J. Biomol. Screening* **2004**, *9* (6), 481–490.
- (15) Schröder, R.; Janssen, N.; Schmidt, J.; Kebig, A.; Merten, N.; Hennen, S.; Müller, A.; Blättermann, S.; Mohr-Andrá, M.; Zahn, S.; Wenzel, J.; Smith, N. J.; Gomeza, J.; Drewke, C.; Milligan, G.; Mohr, K.; Kostenis, E. *Nat. Biotechnol.* **2010**, *28* (9), 943–949.
- (16) Fattinger, C. *Phys. Rev. X* **2014**, *4* (3), 031024.
- (17) Gatterdam, V.; Frutiger, A.; Stengele, K.-P.; Heindl, D.; Lübbers, T.; Vörös, J.; Fattinger, C. *Nat. Nanotechnol.* **2017**, *12*, 1089.
- (18) Frutiger, A.; Blickenstorfer, Y.; Bischof, S.; Forró, C.; Lauer, M.; Gatterdam, V.; Fattinger, C.; Vörös, J. *Phys. Rev. Appl.* **2019**, *11* (1), 014056.
- (19) Midtvedt, D.; Olsén, E.; Höök, F.; Jeffries, G. D. M. *Nat. Commun.* **2019**, *10* (1), 340.
- (20) Ciambrone, G. J.; Liu, V. F.; Lin, D. C.; McGuinness, R. P.; Leung, G. K.; Pitchford, S. J. *Biomol. Screening* **2004**, *9* (6), 467–480.
- (21) Rasmussen, S. G. F.; Choi, H.-J.; Rosenbaum, D. M.; Kobilka, T. S.; Thian, F. S.; Edwards, P. C.; Burghammer, M.; Ratnala, V. R. P.; Sanishvili, R.; Fischetti, R. F.; Schertler, G. F. X.; Weis, W. I.; Kobilka, B. K. *Nature* **2007**, *450* (7168), 383–387.
- (22) Kobilka, B. K.; Dixon, R. A.; Frielle, T.; Dohlman, H. G.; Bolanowski, M. A.; Sigal, I. S.; Yang-Feng, T. L.; Francke, U.; Caron, M. G.; Lefkowitz, R. J. *Proc. Natl. Acad. Sci. U. S. A.* **1987**, *84* (1), 46–50.
- (23) Dohlman, H. G.; Caron, M. G.; Lefkowitz, R. J. *Biochemistry* **1987**, *26* (10), 2657–2664.
- (24) O'Hayre, M.; Eichel, K.; Avino, S.; Zhao, X.; Steffen, D. J.; Feng, X.; Kawakami, K.; Aoki, J.; Messer, K.; Sunahara, R.; Inoue, A.; von Zastrow, M.; Gutkind, J. *Sci. Signal.* **2017**, *10* (484), eaal3395 DOI: 10.1126/scisignal.aal3395.
- (25) Frutiger, A.; Tschannen, C. D.; Blickenstorfer, Y.; Reichmuth, A. M.; Fattinger, C.; Vörös, J. *Opt. Lett.* **2018**, *43* (23), 5801–5804.
- (26) Roed, S. N.; Nøhr, A. C.; Wismann, P.; Iversen, H.; Bräuner-Osborne, H.; Knudsen, S. M.; Waldhoer, M. *J. Biol. Chem.* **2015**, *290* (2), 1233–1243.
- (27) Galés, C.; Rebois, R. V.; Hogue, M.; Trieu, P.; Breit, A.; Hébert, T. E.; Bouvier, M. *Nat. Methods* **2005**, *2* (3), 177–184.
- (28) Atwood, B. K.; Lopez, J.; Wager-Miller, J.; Mackie, K.; Straiker, A. *BMC Genomics* **2011**, *12*, 14.
- (29) Hall, R. A.; Premont, R. T.; Lefkowitz, R. J. *J. Cell Biol.* **1999**, *145* (5), 927–932.
- (30) Yu, N.; Atienza, J. M.; Bernard, J.; Blanc, S.; Zhu, J.; Wang, X.; Xu, X.; Abassi, Y. A. *Anal. Chem.* **2006**, *78* (1), 35–43.
- (31) Giaever, I.; Keese, C. R. *Nature* **1993**, *366* (6455), 591–592.
- (32) Ferguson, S. S. *Pharmacol. Rev.* **2001**, *53* (1), 1–24.
- (33) Luttrell, L. M.; Lefkowitz, R. J. *J. Cell Sci.* **2002**, *115* (3), 455–465.
- (34) Gutkind, J. S.; Kostenis, E. *Nat. Rev. Mol. Cell Biol.* **2018**, *19*, 615.
- (35) Alvarez-Curto, E.; Inoue, A.; Jenkins, L.; Raihan, S. Z.; Prihandoko, R.; Tobin, A. B.; Milligan, G. J. *Biol. Chem.* **2016**, *291* (53), 27147–27159.
- (36) Grundmann, M.; Merten, N.; Malfacini, D.; Inoue, A.; Preis, P.; Simon, K.; Rüttiger, N.; Ziegler, N.; Benkel, T.; Schmitt, N. K.; Ishida, S.; Müller, I.; Reher, R.; Kawakami, K.; Inoue, A.; Rick, U.; Kühl, T.; Imhof, D.; Aoki, J.; König, G. M.; Hoffmann, C.; Gomeza, J.; Wess, J.; Kostenis, E. *Nat. Commun.* **2018**, *9* (1), 341.
- (37) Copik, A. J.; Baldys, A.; Nguyen, K.; Sahdeo, S.; Ho, H.; Kosaka, A.; Dietrich, P. J.; Fitch, B.; Raymond, J. R.; Ford, A. P. D. W.; Button, D.; Milla, M. E. *PLoS One* **2015**, *10* (1), e0115701.
- (38) Pflieger, K. D. G.; Eidne, K. A. *Nat. Methods* **2006**, *3* (3), 165–174.
- (39) Waldhoer, M.; Fong, J.; Jones, R. M.; Lunzer, M. M.; Sharma, S. K.; Kostenis, E.; Portoghese, P. S.; Whistler, J. L. *Proc. Natl. Acad. Sci. U. S. A.* **2005**, *102* (25), 9050–9055.
- (40) Chung, S.; Funakoshi, T.; Civelli, O. *Br. J. Pharmacol.* **2008**, *153* (S1), S339–S346.
- (41) Sugo, T.; Murakami, Y.; Shimomura, Y.; Harada, M.; Abe, M.; Ishibashi, Y.; Kitada, C.; Miyajima, N.; Suzuki, N.; Mori, M.; Fujino, M. *Biochem. Biophys. Res. Commun.* **2003**, *310* (3), 860–868.
- (42) Hay, D. L.; Poyner, D. R.; Sexton, P. M. *Pharmacol. Ther.* **2006**, *109* (1–2), 173–197.
- (43) Levoe, A.; Dam, J.; Ayoub, M. A.; Guillaume, J.-L.; Couturier, C.; Delagrèze, P.; Jockers, R. *EMBO J.* **2006**, *25* (13), 3012–3023.

## Supporting Information

# Quantification of Molecular Interactions in Living Cells in Real Time using a Membrane Protein Nanopattern

Andreas Michael Reichmuth<sup>1</sup>, Mirjam Zimmermann<sup>2</sup>, Florian Wilhelm<sup>2,3</sup>, Andreas Frutiger<sup>1</sup>, Yves Blickenstorfer<sup>1</sup>, Christof Fattinger<sup>4</sup>, Maria Waldhoer<sup>2\*</sup> and János Vörös<sup>1\*</sup>

1 Laboratory of Biosensors and Bioelectronics, Institute of Biomedical Engineering, ETH Zurich, 8092 Zurich, Switzerland

2 InterAx Biotech, PARK innovAARE, 5234 Villigen, Switzerland

3 ETH Zurich, Department of Biosystems Science and Engineering, ETH Zurich, 4058 Basel

4 Roche Pharma Research and Early Development, Roche Innovation Center Basel, 4070 Basel, Switzerland

\*corresponding authors: [janos.voros@biomed.ee.ethz.ch](mailto:janos.voros@biomed.ee.ethz.ch), [waldhoer@interaxbiotech.com](mailto:waldhoer@interaxbiotech.com)

<b>Supporting Information</b>	<b>S1</b>
Figure S1: RIL process for template mologram generation	S2
Figure S2: Establishment of intracellular mologram	S3
Figure S3: NECA control on EPAC sensor	S4
Figure S4: cAMP formation in arrestin devoid cells	S4
Figure S5: Dose curves for Isoproterenol and Formoterol	S5
<b>Supporting Materials &amp; Methods</b>	<b>S6</b>
Cell lines	S6
Real-time cAMP assays	S6
Data analysis	S7
<b>Supporting references</b>	<b>S7</b>

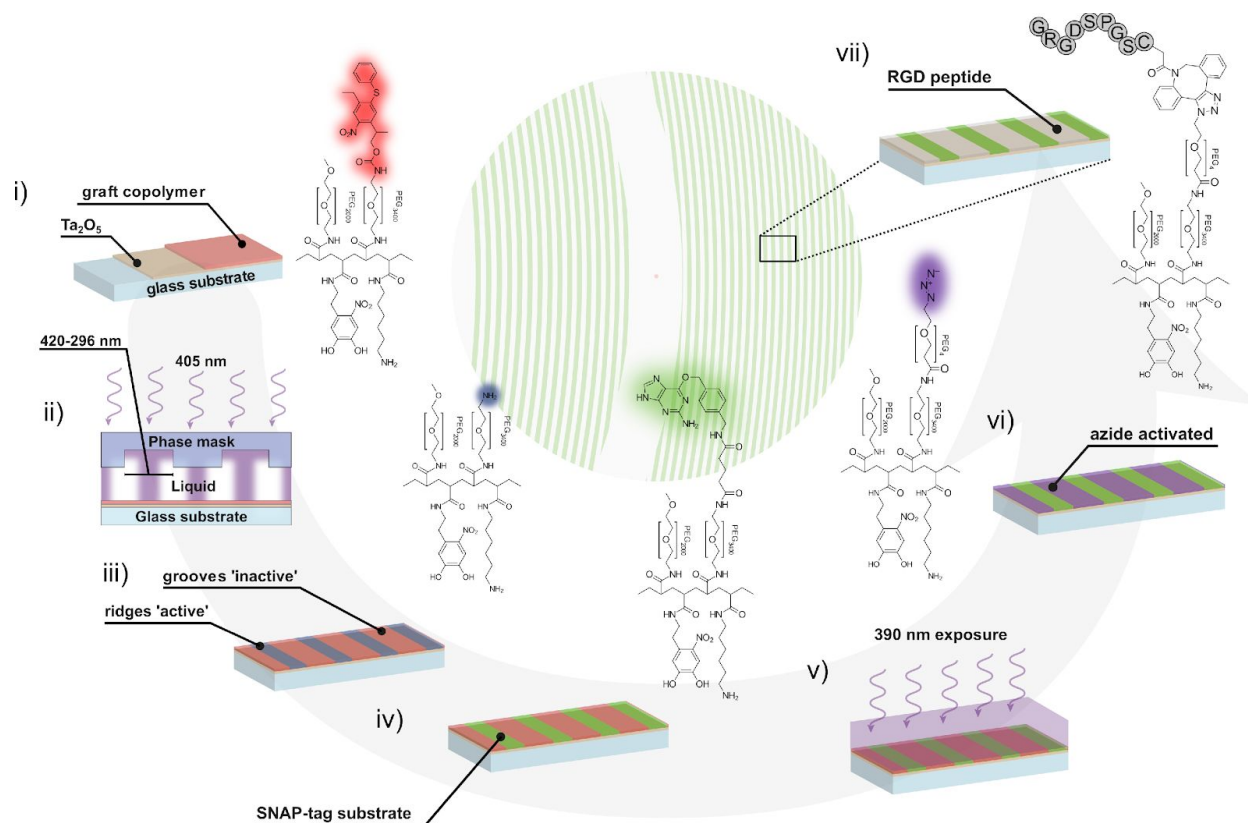


**Figure S1: RIL process for template mologram generation.** In order to generate the affinity modulation required for focal molography, a Ta<sub>2</sub>O<sub>5</sub> single-mode waveguide is coated with a photoprotected PAA-g-PEG copolymer (i). RIL was used for the preparation of molograms. Thereby, the copolymer is illuminated through a Ta<sub>2</sub>O<sub>5</sub> phase mask using a 405 nm solid state laser to deprotect the reactive groups (ii). After phase mask illumination primary amines are obtained on the ridges of the molographic pattern (iii). The ridges can be functionalized using amine reactive NHS-chemistry such as the SNAP-tag substrate NHS-BG-GLA (iv). Flood exposure at 390 nm with a dose of 1200 mJ/cm<sup>2</sup> is used to remove the remaining photoprotective groups in the grooves (v)<sup>1</sup>. The primary amines are then functionalized with a hetero-bifunctional crosslinker for bio-orthogonal strain promoted azide-alkyne cycloaddition (vi). The RGD containing peptides, facilitating adhesion of cells to the chip, are then covalently immobilized to the grooves (vii).

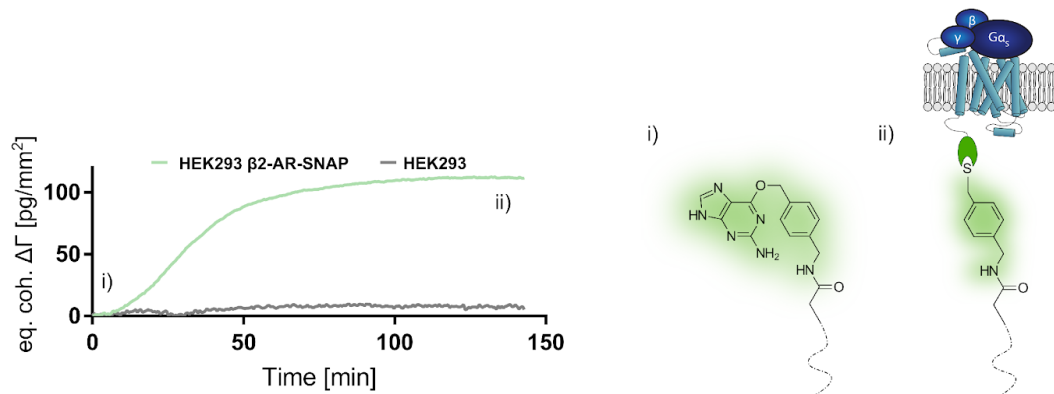


**Figure S2: Establishment of transmembrane mologram.** HEK293 cells overexpressing SNAP-β2AR are added to the sensor chip (i, green curve and cartoon) which allows the auto-reactive SNAP-tag on the extracellular side of the β2ARs to covalently bind the template mologram (ii, green curve and cartoon). Thereby, a transmembrane mologram is established (green curve). On the other hand, endogenous proteins in wild type HEK293 cells do not establish a transmembrane mologram and thus do not contribute to the signal (grey curve). Data shows the equivalent coherent mass modulation of the mologram.

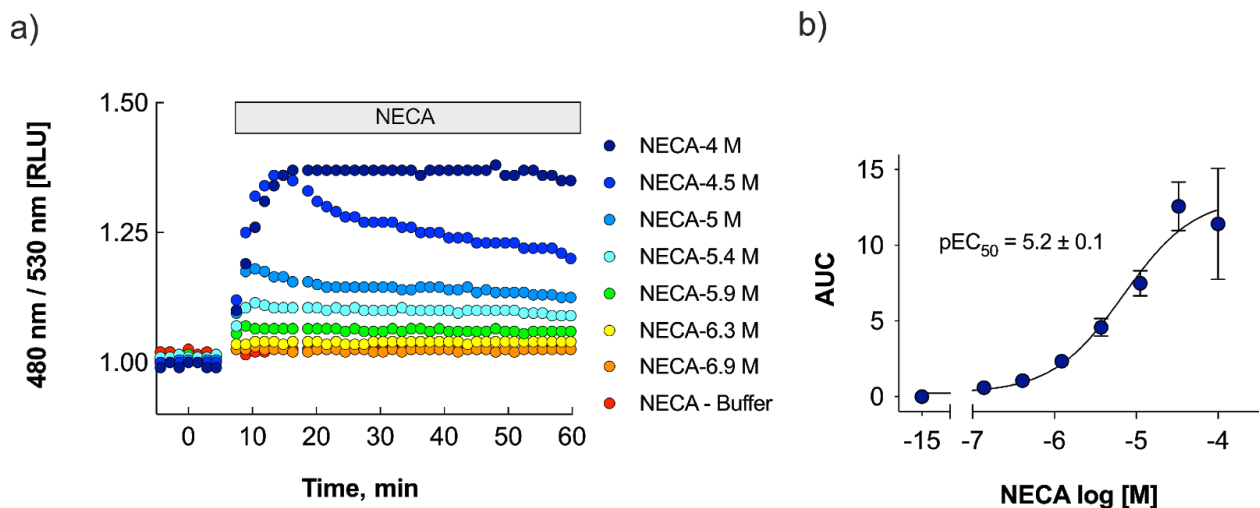


**Figure S3: a) Time-course of NECA-induced cAMP formation.** Formation of cAMP is measured in HEK293 cells stably expressing the EPAC FRET-sensor. EPAC HEK293 cells were stimulated with increasing concentrations of NECA. The EPAC FRET ratio mCerulean/mCitrine (480 nm/530 nm) was plotted as a function of time. Data represent one representative out of three independent experiments carried out in duplicates.

**b) Concentration-response curve of NECA-induced cAMP formation.** Concentration-response curve of NECA-induced cAMP formation in EPAC HEK293 cells. The area under the curve (AUC) was plotted as a function of the NECA concentrations. Data represent mean  $\pm$  s.d. of three individual experiments carried out in duplicates.

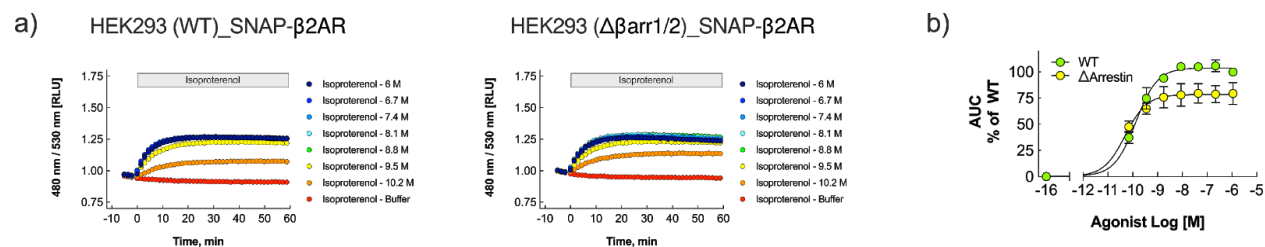


**Figure S4: a) Time-course of Isoproterenol-induced cAMP formation.** Formation of cAMP is measured in WT (left) or  $\Delta\beta$ arr1/2 (right) HEK293 cells stably expressing SNAP-β2AR and the EPAC FRET-sensor. SNAP-β2AR-EPAC HEK293 cells were stimulated with increasing concentrations of Isoproterenol. The EPAC FRET ratio mCerulean/mCitrine (480 nm/530 nm) was plotted as a function of time. Data represent one representative out of three independent experiments carried out in duplicates.

**b) Concentration-response curves of Isoproterenol-induced cAMP formation.** Concentration-response curves of Isoproterenol-induced cAMP formation in WT and  $\Delta\beta$ arr1/2 SNAP-β2AR-EPAC HEK293 cells. The area under the curve (AUC) was plotted as a function of the Isoproterenol concentrations. Data represent mean  $\pm$  s.d. of three individual experiments carried out in duplicates.

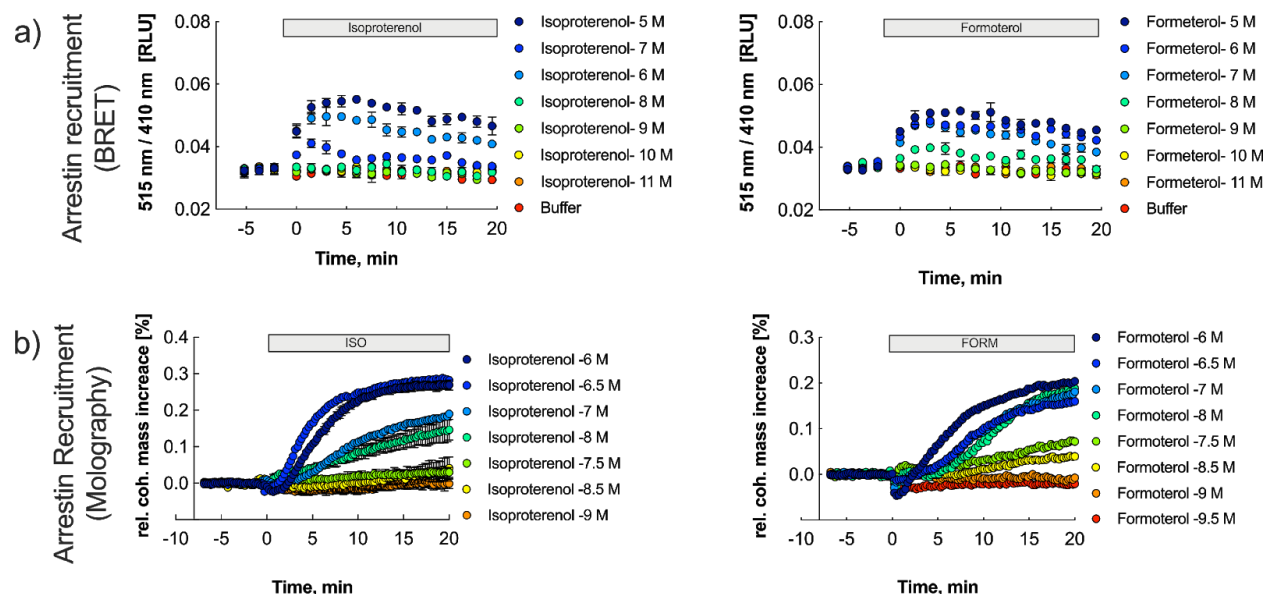


**Figure S5: a) Time-course of Isoproterenol and Formoterol-induced recruitment of  $\beta$ arr2 to  $\beta$ 2AR.** HEK293 cells transiently co-expressing  $\beta$ 2AR-RLuc8 and GFP- $\beta$ arr2 constructs were treated with Coelenterazine 400A and stimulated with increasing concentration of Isoproterenol (left) or Formoterol (right). Recruitment of the GFP-tagged  $\beta$ arr2 constructs to  $\beta$ 2AR-RLuc8 was detected through measuring the BRET signal as described in the Methods section. Representative data of one out of four independent experiments measured in duplicates are shown.

**b) Real-time molographic measurements of Isoproterenol and Formoterol-induced arrestin recruitment to  $\beta$ 2AR.** Arrestin recruitment to  $\beta$ 2ARs was measured in HEK293 cells stably expressing SNAP- $\beta$ 2ARs. Cells were incubated on the molographic chip and subsequently stimulated with increasing concentrations of Isoproterenol (left) and Formoterol (right). The molographic signal is plotted as a concentration dependent fractional increase compared to baseline.

## Supporting Materials & Methods

### Cell lines

The SNAP- $\beta$ 2AR cell line in a HEK293 background stably expressing the EPAC-cAMP sensor with mCerulean and mCitrine as FRET pair, further referred to as SNAP- $\beta$ 2AR-EPAC, was generated by transfecting a SNAP- $\beta$ 2AR plasmid into a cell line stably expressing the EPAC-cAMP sensor using Lipofectamine 2000<sup>2</sup>. SNAP- $\beta$ 2AR-EPAC clones were selected by cultivating the cells in DMEM containing 10% FCS, 2 mg/ml G418 and 0.06 mg/ml zeocin in a humidified 5% CO<sub>2</sub> air incubator at 37°C.

### Real-time cAMP assays

To measure the accumulation of cAMP upon stimulation of the  $\beta$ 2AR, a cAMP assay was performed as previously described<sup>3,4</sup>. SNAP- $\beta$ 2AR-EPAC cells were seeded at a density of 50'000 cells/well in sterile, black 96-well microplates coated with poly-L-lysine and cultured overnight. Cells were incubated in 80  $\mu$ l HBSS (supplemented with 20 mM HEPES, pH 7.4) in darkness for 15 min prior to stimulation with Isoproterenol or Formoterol in the concentrations indicated at RT. Excitation of the EPAC donor (mCerulean) with 10 flashes (flash lamp) per well at 430 nm and emission measurement of the EPAC donor and the EPAC acceptor respectively (mCitrine) was performed with a dual emission fluorescence optical module (FI 430 530 480) using a PHERAstar FSX from BMG Labtech (Ortenberg, Germany). mCerulean/mCitrine ratios were normalized to 1  $\mu$ M Isoproterenol and plotted as a function of time for 40 min post stimulation.

### Data analysis

For the cAMP assay the concentration-response curves with area under the curve (AUC) vs. ligand concentrations were fitted using the nonlinear regression “log(inhibitor) vs. response (three parameters)” in GraphPad Prism to calculate the pIC<sub>50</sub> values.

## Supporting references

- (1) Gatterdam, V.; Frutiger, A.; Stengele, K.-P.; Heindl, D.; Lübbers, T.; Vörös, J.; Fattinger, C. Focal Molography Is a New Method for the in Situ Analysis of Molecular Interactions in Biological Samples. *Nat. Nanotechnol.* **2017**. <https://doi.org/10.1038/nnano.2017.168>.
- (2) Mathiesen, J. M.; Vedel, L.; Bräuner-Osborne, H. cAMP Biosensors Applied in Molecular Pharmacological Studies of G Protein-Coupled Receptors. *Methods Enzymol.* **2013**, *522*, 191–207.
- (3) Roed, S. N.; Wismann, P.; Underwood, C. R.; Kulahin, N.; Iversen, H.; Cappelen, K. A.; Schäffer, L.; Lehtonen, J.; Hecksher-Soerensen, J.; Secher, A.; Mathiesen, J. M.; Bräuner-Osborne, H.; Whistler, J. L.; Knudsen, S. M.; Waldhoer, M. Real-Time Trafficking and Signaling of the Glucagon-like Peptide-1 Receptor. *Mol. Cell. Endocrinol.* **2014**, *382* (2), 938–949.
- (4) Vedel, L.; Bräuner-Osborne, H.; Mathiesen, J. M. A cAMP Biosensor-Based High-Throughput Screening Assay for Identification of Gs-Coupled GPCR Ligands and Phosphodiesterase Inhibitors. *J. Biomol. Screen.* **2015**, *20* (7), 849–857.